AKADÉMIAI KIADÓ

UNIVERSITY of DEBRECEN

International Review of Applied Sciences and Engineering

14 (2023) 3, 303–315

DOI:
10.1556/1848.2023.00524

ORIGINAL RESEARCH PAPER

Direct expansion (DX) air conditioning (A/C) system control: Hybrid BOANFIS technique

Seema Haribahu Jadhav* and Rajashree Vilas Sarwadnya

Department of Instrumentation Engineering, Shri Guru Gobind Singhji Institute of Engineering and Technology, (SGGS I E&T), Vishnupuri, Nanded, Maharashtra - 431 606, India

Received: May 19, 2022 • Accepted: February 5, 2023
Published online: April 19, 2023

ABSTRACT

This paper describes a novel hybrid technique with fractional order PID controller (FOPID) for simultaneously controlling the humidity of indoor air temperature and the direct expansion (DX) air conditioning (A/C) system. The proposed hybrid system is a joint performance of the butterfly optimization algorithm (BOA) and adaptive network fuzzy inference system (ANFIS), hence forth it is called BOANFIS Technique (BOANFIST). The purpose of the proposed system is to disconnect the temperature and humidity control circuits. The proposed control is modeled and replicated on MATLAB platform and is assessed using existing systems. The statistical performance of the proposed and existing systems of mean, median and standard deviation is also evaluated. It reduces computational time up to 1.01 s and also reduces energy consumption to around 16.42 KWh/day. Furthermore, the simulation outcomes suggest that the proposed technique may efficiently and accurately obtain the optimal global solutions of the proposed technique compared to existing systems.

KEYWORDS

direct expansion (DX) air conditioning (A/C) system, fractional order PID controller (FOPID), temperature and humidity control

1. INTRODUCTION

In buildings, it is significant to control indoor humidity at a suitable level, because it directly affects building owners' thermal comfort, indoor air quality (IAQ), with operational ability to build air conditioning installations [1]. Several humidity control techniques, heat pipe technology and outside air pre-conditioning [2] have been formulated for huge central A/C systems not appropriate for DX A/C systems [3]. Despite that, a large amount of DX A/C systems are presently fitted through single speed compressor as well as fans, which rely on cycling on and off to keep only the interior temperature of the dry lamp. This outcome is uncontrolled balance indoor humidity, which leads to thermal discomfort, poor IAQ with less energy efficiency for residents [4].

The variable frequency inverters are generally enabled the distribution fan in a DX A/C system, creating a novel method to concurrently control RH and indoor air temperature using DX A/C systems [5]. Nevertheless, complex dynamic heat with mass transfer properties that occur on variable-speed DX air conditioning systems make it very hard for enlarging a control system for instantaneous control of indoor air humidity and temperature [6–8]. For instance, due to great cross-coupling among two feedback loops, which is due to the variation of the compressor that produces the temperature control, and because the variation of speed of supply fan produces a humidity control, DX air conditioning systems variable speed drives that have conventional PID feedback controller is insufficient [9–12].

Whereas the DX A/C system is an inside evaporator, heat and mass shift among air and refrigerant could be appraised using an elaborate physical model, hence it is necessary for decoupling two coupled control loops [13–20]. However, the heat and mass shift of DX evaporator affects a huge number of factors consisting of heat and fluid flow geometry, flow

*Corresponding author.
E-mail: seema_keshav@yahoo.co.in

AKJournals

turbulence, and so on. [21]. If physical model is produced for DX cooling with dehumidification coil, hence, it is practically not possible to take all of these elements [22]. Based on the assumption of Lewis unit number, the mass shift coefficient is appraised as heat transfer coefficient. However, many reported studies suggest that the Lewis number deviates as being one. Furthermore, the improvement of a controller based on physical models is necessary [23–25]. To overwhelm the issues, the novel system for DX A/C system is essential. The proposed approach optimally controls air temperature as well as humidity through better accuracy and less computation time.

The rest of paper is declared as follow: Section 2 describes the literature review of the current work, Section 3 explains the system modeling and design, Section 4 clarifies proposed optimization. Section 5 describes result and discussion. Finally, section 6 finishes the manuscript.

2. RECENT RESEARCH WORK

Numerous investigation works can be found in the literature that relied on optimal PID controller design for DX A/C system with dissimilar systems and aspects. Some of the work is reviewed.

Xia et al. [26] have established hunting results on the poor operational safety and performance of DX A/C system; when it is variable speed (VS) operated to dissimilar sensible and latent cooling capabilities. The obtainable dynamic design was more formulated by involving equations to estimate temperature sensor dynamics and wind side motion parameters. Sholahudin et al. [27] have illustrated the determination of dynamic effectiveness for DX A/C system that was advanced by Bayesian artificial neural network (ANN). Input and output data sets were created via changing the compressor speed at different signal amplifiers by a dedicated AC simulator and containing dynamic cooling load with ambient temperature. Energy dissipation that refers to potential losses at work in system and selected as ambient temperature output variables for thermal comfort. The key specification of the ANN design, which contains the number of neurons and latency lines, were optimized to improve the prediction accuracy.

For enhancing the DX A/C system designed air flow rate of 20,000 m^3/h, design concept of split front evaporator by modernized suction head and suffocation on capillaries was adopted and the design explained by Tang et al. [28]. DX A/C system design was experimented and verified on a trial basis. The front split decreased the cooling pressure drop at evaporator suction head and suffocation design restricted the maximal flow rate in every branch circuit, helping to improve the cooling flow distribution of system.

Xie et al. [29] have executed the occupant behavior (OB), which was identified as an important factor influencing the energy consumption of a building's occupants. Air conditioning application and aggression simulation technique; It integrate OB design with Energy Plus (E+) modified distributed air conditioning system. Initially, we created an observation system, which utilizes motion sensors with thermostats for measuring the utilization and usefulness of air conditioning in a hotel building.

Yan et al. [30] have illustrated short to medium size buildings; DX A/C systems were highlighted applications. Multi-variable Controller (MVC) was established for DX Variable Speed (VS) air conditioning systems. Yan et al. [31] have executed the primary A/C uses offering occupants acceptable levels of interior thermal comfort and six parameters. Despite that many A/C systems only control air temperature. Any time five non-temperature parameters differ remarkably, a resident may feel hot and uncomfortable. For solving the problem, a full thermal comfort index must be utilized to regulate A/C systems; a fuzzy logic controller was obtained. However, the fuzzy logic control method was complex and then the previously installed fuzzy logic driver was interpreted for its actual use.

Chen et al. [32] have introduced the conventional on-off control single evaporator DX A/C system; it must operate under various seasonal cooling load conditions. Therefore, it would be difficult to try to maintain a different indoor temperature environment the entire time if not complex and costly ancillary activities provide different dehumidification capabilities.

2.1. Background of the research work

A review of the current research work displays that the operation and control of an air conditioning system is always a challenging and difficult task. A TEV features and the nonlinearity of evaporator superheat. Hunting also causes a lack of safety and operational efficiency of the DX A/C system. Various approaches such as Markov Chain method, Artificial Neural Network (ANN), Monte-Carlostochastic Model and Fuzzy Logic Controller (FLC) are used in air condition system stability. The ANN approach is utilized for dynamic performance recognition in DX AC system and the drawbacks of ANN hardware are dependence, inexplicable characteristics of appropriate network structure and complexity of displaying the trouble. Therefore, the outcomes are perceived dependent on the assumption; hence it may not be extensively accepted. However, studies on the investigation of temperature sensor dynamics with air side operating features cannot be recognized. To overcome these challenges, optimal DX system control is required. A/C using advanced hybrid technology. In the literature, numerous works are presented to solve this problem and the presented papers do not provide efficient outcomes. These problems have inspired the present investigation work.

3. DIRECT EXPANSION AIR CONDITIONING (DX-A/C) SYSTEM

Figure 1 illustrates the schematic diagram of the DX A/C system. It consists of two portions, i.e., DX refrigeration and air distribution subsystem. The DX refrigeration plant comprises of electronic expansion valve (EEV), changeable speed compressor, DX condenser and evaporator. The DX

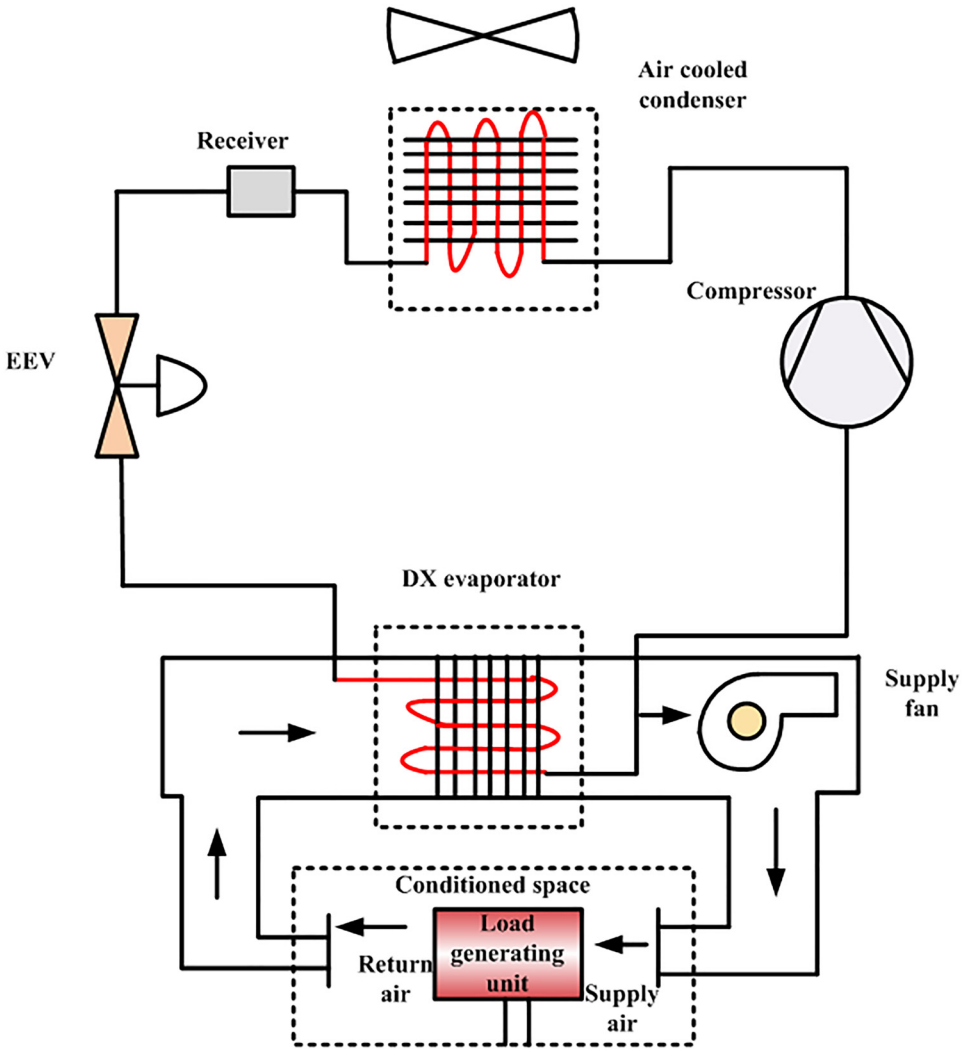

Fig. 1. Schematic diagram of DX-A/C system

plant thermodynamic cycle contains the processes of isenthalpic expansion, isentropic compression, rejection and condensation of isobaric heat, and processes of evaporation and absorption of isobaric heat [33]. The evaporator DX was located in the air supply pipe to act as an air cooling coil. Moreover, EEV incorporates a pulse generator, a step motor and a throttle needle valve that is utilized for preserving the superheat degree of refrigerant in evaporator outlet. Besides, condenser cooling air is utilized by condenser air duct for conduction that carries unwanted heat as condenser to the outside of the laboratory. Cooling air temperature input into the condenser is utilized by electric heater that is controlled via solid state relay (SSR). Furthermore, the air distribution subsystem integrated an air distribution duct network by changeable speed centrifugal supply fan; returns air dampers with conditioned space [34].

3.1. Dynamic model of DX A/C system

Depending on energy and mass conservation, the DX A/C system dynamic model is exposed. The following assumptions are taken for the DX A/C mathematical modeling system [35].

- 25% fresh air is permitted to enter the system and it mixes with 75% re-circulated air in the evaporator.
- Inside the heat exchangers, adequate air mixing takes places in which air is conditioned.
- DX evaporator air side may be separated into two areas, i.e., dry and wet-cooling region; in region of dry-cooling, the air temperature is diminished and the dehumidification occurs mainly in the wet-cooling area.
- In air ducts, the thermal losses are neglected.
- Air conditioning in the room is extracted using a fan; up to 75% of air is re-circulated and remaining air is blown out of the system through a fan.

DX A/C system mass and energy conservation equations may be illustrated as follows depending on the above considerations [36]. The energy balance equation model for conditioned space temperature is expressed in Eq. (1):

$$C_{sa}\delta V^{*}\frac{dT_{cs}^{*}}{dt}=C_{sa}\delta V_{f}^{*}\left(T_{e}^{*}-T_{cs}^{*}\right)+Q_{l}^{*}+k_{s}V_{f}^{*} \quad (1)$$

where V_f^* denotes volumetric air flow rate, C_{sa} implies air specific heat, δ is the moisture air density, Q_l^* denotes sensible load of the space, k_s implies supply fan heat gain coefficient, T_e^* is air leaving DX cooling coil temperature, and T_{cs}^* denotes temperature of air in conditioned space. Volumetric air flow rate is illustrated in Eq. (2):

$$V_{f}^{*}=k_{f}^{*}S_{f}^{*} \quad (2)$$

where k_f^* implies supply fan speed coefficient, S_f^* implies speed of supply fan. Sensible load of space Q_l^* is generally related to the electrical devices and residents. According to the electrical device characteristics, heat emitted from electric devices is simple to recognize; because the load linked to occupant that may be modeled via current concentration of CO_2 in conditioning room [37]. Sensible heat load Q_l^* may be modeled using Eq. (3):

$$Q_{l}^{*}=\mu C_{c}^{*}+\nu \quad (3)$$

where C_c^* is the concentration of CO_2 in the room, μ and ν denotes gain parameters of sensible heat. The mass conservation of dynamic mathematical model of moisture within the conditioned space is denoted in Eq. (4):

$$\delta V^{*}\frac{dW_{cs}^{*}}{dt}=C_{sa}\delta V_{f}^{*}\left(W_{e}^{*}-W_{cs}^{*}\right)+M^{*} \quad (4)$$

where M^* implies production of moisture load on conditioned space, W_e^* is air leaving the DX cooling coil moisture content, W_{cs}^* is moisture of the air in conditioned space. The principle of conservation of energy on air side of the dry-cooling region is calibrated using Eq. (5):

$$C_{sa}\delta V_{h1}^{*}\frac{dT_{d}^{*}}{dt}=C_{sa}\delta V_{f}^{*}\left(T_{cs}^{*}-T_{d}^{*}\right)+\beta_{1}A_{1}\left(T_{w}^{*}-\frac{T_{cs}^{*}+T_{d}^{*}}{2}\right) \quad (5)$$

where T_w^* is the evaporator wall of the DX air temperature, β_1 is coefficient of the heat transfer [38]. The energy balance region of wet-cooling because of the powerful combination between moisture and temperature can be demonstrated in Eq. (6):

$$\begin{aligned}C_{sa}\delta V_{h2}^{*}\frac{dT_{e}^{*}}{dt}+\delta V_{h2}^{*}\frac{dW_{e}^{*}}{dt}&=C_{sa}V_{f}^{*}\left(T_{d}^{*}-T_{e}^{*}\right)\\&+\delta V_{f}^{*}h_{fg}^{*}\left(W_{cs}^{*}-W_{e}^{*}\right)\\&+\beta_{2}A_{2}\left(T_{w}^{*}-\frac{T_{d}^{*}+T_{e}^{*}}{2}\right)\end{aligned} \quad (6)$$

where A_2 implies DX evaporator heat transfer region of wet-cooling, V_{h2}^* is DX evaporator volume in air side on wet-cooling region on air side, h_{fg}^* implies water vaporization latent heat and β_2 implies coefficient of the heat transfer. A dynamic mathematic model through the energy equation conservation for evaporator wall is denoted in the following equation:

$$\begin{aligned}\left(C_{sa}\delta V^{*}\right)_{w}\frac{dT_{w}^{*}}{dt}&=\beta_{1}A_{1}\left(\frac{T_{cs}^{*}+T_{d}^{*}}{2}-T_{w}^{*}\right)\\&+\beta_{2}A_{2}\left(\frac{T_{d}^{*}+T_{e}^{*}}{2}-T_{w}^{*}\right)\\&-M_{ref}^{*}\left(h_{r2}^{*}-h_{r1}^{*}\right)\end{aligned} \quad (7)$$

$$M_{mf}^{*}=\frac{V_{sc}^{*}V_{\mathrm{com}}^{*}}{V_{s}^{*}}\gamma=\frac{V_{sc}^{*}V_{\mathrm{com}}^{*}}{V_{s}^{*}}\left(1-0.015\left[\left(P_{c}^{*}/P_{e}^{*}\right)^{1/\alpha}\right]\right) \quad (8)$$

where M_{mf}^* implies refrigerant mass flow rate, V_{sc}^* is compressor speed, γ is coefficient of compressor displacement, α refers to the index of compressor that is considered as a constant at the value of 1.18, V_s^* is the superheated refrigerant specific volume, h_{r1}^* and h_{r2}^* denote refrigerant enthalpy, P_c^* and P_e^* refer to the pressure of condensing and evaporating and V_{com}^* is the rotor compressor swept volume. The relationship between temperature and humidity can be expressed as

$$\frac{dW_{e}^{*}}{dt}=\frac{2\times0.0198T_{e}^{*}+0.085}{1000}\frac{dT_{e}^{*}}{dt} \quad (9)$$

$$\dot{Y}=f(Y,U)=D^{-1}f_{1}(Y,U)+D^{-1}f_{2}(X) \quad (10)$$

where $\dot{Y}=[T_e^*, T_d^*, T_w^*, T_{cs}^*, W_{cs}^*, W_e^*], U=[V_f^*, V_{sc}^*]^T$ and $Z=[Q_{\mathrm{old}}^*, M^*]^T$.

$$f_{1}(y,u)=\left[f_{11}f_{12}f_{13}f_{14}f_{15}0f_{17}\right] \quad (11)$$

$$f_{11}=_{sa}\delta V_{f}^{*}\left(T_{e}^{*}-T_{cs}^{*}\right)+\mu C_{c}^{*}+k_{s}V_{f}^{*} \quad (12)$$

$$f_{12}=C_{sa}\delta V_{f}^{*}h_{fg}^{*}\left(W_{e}^{*}-W_{cs}^{*}\right)+\mu C_{c}^{*} \quad (13)$$

$$f_{13}=C_{sa}\delta V_{f}^{*}\left(T_{cs}^{*}-T_{d}^{*}\right)+\beta_{1}A_{1}\left(T_{w}^{*}-\frac{(1-p)T_{cs}^{*}+pT_{d}^{*}}{2}\right) \quad (14)$$

$$\begin{aligned}f_{14}&=C_{sa}\delta V_{f}^{*}\left(T_{d}^{*}-T_{e}^{*}\right)+\delta V_{f}^{*}h_{fg}^{*}(1-p)W_{cs}^{*}+pW_{0}^{*}-W_{e}^{*}\Big)\\&+\beta_{2}A_{2}\left(T_{w}^{*}-\frac{T_{d}^{*}+T_{e}^{*}}{2}\right)\end{aligned} \quad (15)$$

$$\begin{aligned}f_{15}&=\beta_{1}A_{1}\left(\frac{(1-p)T_{cs}^{*}+T_{d}^{*}+pT_{0}^{*}}{2}-T_{w}^{*}\right)\\&+\beta_{2}A_{2}\left(\frac{T_{d}^{*}+T_{e}^{*}}{2}-T_{w}^{*}\right)\\&-M_{mf}^{*}\left(h_{r2}^{*}-h_{r1}^{*}\right)\end{aligned} \quad (16)$$

$$f_{17}=V_{c}^{*}\left(C_{0}^{*}-C_{c}^{*}\right) \quad (17)$$

$$f_{2}(x)=\left[\mu\quad\nu\quad0\quad0\quad0\quad0\quad GP\right]^{T} \quad (18)$$

Decoupling matrix D^* is estimated using Eq. (19):

$$D^* = \begin{bmatrix} 0 & C_{sa}\delta V^* & 0 & 0 & 0 & 0 & 0 \\ 0 & 0 & 0 & 0 & 0 & \delta V^* h^*_{fg} & 0 \\ 0 & 0 & C_{sa}\delta V^*_{h1} & 0 & 0 & 0 & 0 \\ C_{sa}\delta V^*_{h2} & 0 & 0 & 0 & 0 & 0 & 0 \\ 0 & 0 & 0 & C_{sa,w}\delta_w V^*_w & \delta V^*_{h2} h^*_{fg} & 0 & 0 \\ -\dfrac{2\times 0.0198 T^*_e + 0.085}{1000} & 0 & 0 & 0 & 1 & 0 & 0 \\ 0 & 0 & 0 & 0 & 0 & 0 & V^* \end{bmatrix} \quad (19)$$

DX-A/C system dynamic model is established by evaluation technique for model parameter recognition with satisfactory accuracy.

4. CONTROL STRATEGY

The system response creates the damping oscillation and the steady state error. Fractional calculus is expansion of fractional orders integration and differentiation for FOPID controller, which is represented in Eq. (20) [39].

$${}_bD^{\alpha}_t = \begin{cases} \dfrac{d^{\alpha}}{dt^{\alpha}} & \alpha>0 \\ 1 & \alpha = 0 \\ \displaystyle\int_0^t dt^{\alpha} & \alpha<0 \end{cases} \quad (20)$$

$$\alpha - 1 \le \alpha \le \kappa \quad (21)$$

The differential equation of a FOPID controller is defined in Eq. (22):

$$u(t) = k^*_p e(t) + k^*_i d_t^{-\lambda} e(t) + k^*_d d_t^{\delta} e(t) \quad (22)$$

$$G^*_c(s) = k^*_p + k^*_i s^{-\lambda} e(t) + k^*_d S^{\delta} \quad (23)$$

The process result is in accordance with the reference on steady state and comprehensiveness is assured. A steady state is assumed for balancing control signal u_o constant error $e_o \neq 0$.

$$u_0 = k_p e_0 + k_i e_0 t \quad (24)$$

$$u = k_p e + \frac{1}{1+sT} u \quad (25)$$

$${}_bD^{\alpha}_t f(t) = \frac{1}{\Re(\kappa-\alpha)} \int_b^t \frac{f^{\alpha}(\tau)}{(t-\tau)^{\alpha-\kappa+1}} d\tau \quad (26)$$

$$u(t) = k_p e(t0) + k_d \frac{de}{dt} = k_p \left[e(t) + T_d \frac{de}{dt} \right] = k_p e_p(t) \quad (27)$$

where the derivation time refers to $T_d = k_d/_d$.

$$O.F = Min\left(\sum\nolimits_{s=1}^{4} J_s \right) \quad (28)$$

$$J_1 = IAE(Integral\ Absolute\ Error) = \int_0^{\infty} |e(t)| dt \quad (29)$$

$$J_2 = ISE(Integral\ Square\ Error) = \int_0^{\infty} \left| e^2(t) \right| dt \quad (30)$$

$$J_3 = ITAE(Integral\ with\ Time\ Absolute\ Error) = \int_0^{\infty} t|e(t)| dt \quad (31)$$

$$J_4 = ITSE(Integral\ with\ Time\ Square\ Error) = \int_0^{\infty} te^2(t) dt \quad (32)$$

Subjected with,

$$k_p^{\min} < k_p < k_p^{\max} \quad (33)$$

$$k_i^{\min} < k_i < k_i^{\max} \quad (34)$$

$$k_d^{\min} < k_d < k_d^{\max} \quad (35)$$

$$\lambda^{\min} < \lambda < \lambda^{\max} \quad (36)$$

$$\mu^{\min} < \mu < \mu^{\max} \quad (37)$$

For estimating the necessary sensible capacitance $Q_{s,E}$, and latent capacitance $Q_{l,E}$, $T_{d,b}$ and $T_{w,b}$ are considered as the two inputs of controller. The necessary sensible capacitance $Q_{s,E}$, and latent capacitance $Q_{l,E}$ may be predicted.

$$Q_{s,E} = \sum\nolimits_{i=1}^{n} P_{lv}(\Delta T_{dbi}) \times W_{lv}(\Delta T_{dbi}) + P_{lv}(\Delta T_{dbi}) \times \sum\nolimits_{j=1}^{n} P_{lv}\left(\partial T_{dbj}\right) \times W_{lv}\left(\partial T_{dbj}\right) \quad (38)$$

$$Q_{l,E} = \sum\nolimits_{i=1}^{n} P_{lv}(\Delta T_{wbi}) \times W_{lv}(\Delta T_{wbi}) + P_{lv}(\Delta T_{wbi}) \times \sum\nolimits_{j=1}^{n} P_{lv}\left(\partial T_{wbj}\right) \times W_{lv}\left(\partial T_{wbj}\right) \quad (39)$$

where P_{lv} is the linguistic variable probability, W_{lv} linguistic variable weight, T_{dbi} implies temperature of air dry-bulb in °C, and T_{wbi} implies temperature of the air wet-bulb in °C. The entire outcome cooling capacity is denoted in Eq. (40):

$$Q_{t,E} = Q_{s,E} + Q_{l,E} \tag{40}$$

$$SHR_E = Q_{s,E}/Q_{l,E} \tag{41}$$

The FOPID controller parameter may be tuned by the BOANFIS system, which manages the indoor humidity and air temperature. The proposed control strategy schematic diagram is portrayed in Fig. 2.

4.1. Proposed BOANFIST to control indoor air temperature and humidity

The proposed hybrid system is known as the BOANFIS Technique because it combines the Butterfly Optimization Algorithm (BOA) and the ANFIS; hence it is called (BOANFIST). A butterfly can produce the fragrance by several intensities that are interrelated by their fitness [40]. While a butterfly is capable to smell the fragrance of other butterfly, it would travel on a global search. Five layers are shown on ANFIS. Every layer has certain nodes on node function; (a) Fuzzification method; (b) Fuzzy of last piece; (c) Normalization functions membership; (d) Fuzzy rules of resultant piece; (e) Network exit. For deciding the parameters of fuzzy inference system on ANFIS structure of Sugeno hybrid training algorithm is used. For creating as well as organizing the parameter units of membership functions in fuzzy inference system, the algorithm combines least squares methods as well as the BP gradient descent algorithm [41].

4.1.1. Step by step method of hybrid BOANFIS method. The indoor air dry-bulb temperature $T_{d,b}$ and wet-bulb temperature $T_{w,b}$ are taken as input parameters of the BOA technique. After initiation method, the input parameters are randomly created. Then the controller parameter FOPID is adjusted via ANFIS system. The comprehensive step method is clarified below,

Step 1: Initiation

Initialize state, disturbance and control vector $X = [x_1, x_2, \ldots x_n]$, $Y = [y_1, y_2, \ldots y_n]$ and $C = [c_1, c_2, \ldots c_n]$ of DX-A/C system.

Step 2: Random generation

Initialize BOANFIST optimization as X_j *for* $j = 1, 2, 3, \ldots, m$. The data gain parameters K_p, K_i and K_d are engaged as input that is arbitrarily created by below matrix Z:

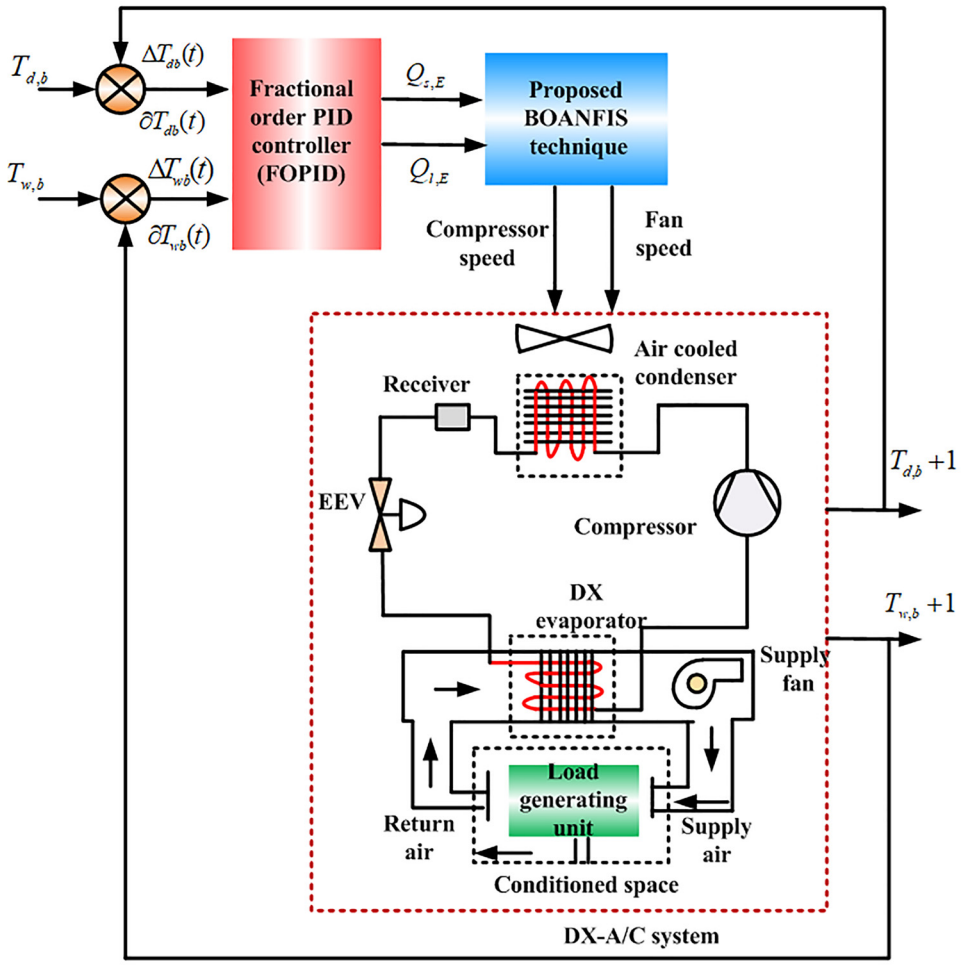

Fig. 2. Schematic diagram of control strategy

$$Z = \begin{bmatrix} K_p^{11}K_i^{11}K_d^{11}\lambda^{11}\mu^{11} \; K_p^{12}K_i^{12}K_d^{12}\lambda^{12}\mu^{12} \; \ldots \; K_p^{1m}K_p^{1m}K_d^{1m}\lambda^{1m}\mu^{1m} \\ K_p^{21}K_i^{21}K_d^{21}\lambda^{21}\mu^{21} \; K_p^{22}K_i^{22}K_d^{22}\lambda^{22}\mu^{22} \ldots \; K_p^{2m}K_i^{2m}K_d^{2m}\lambda^{2m}\mu^{2m} \\ \vdots\vdots\vdots \\ K_p^{n1}K_i^{n1}K_d^{n1}\lambda^{n1}\mu^{n1} \; K_p^{n2}K_i^{n2}K_d^{n2}\lambda^{n2}\mu^{n2} \; \ldots K_p^{nm}K_i^{nm}K_d^{nm}\lambda^{nm}\mu^{nm} \end{bmatrix} \tag{42}$$

Step 3: Fitness Function

The fitness of DX-A/C system is computed as below,

$$F_t = \begin{bmatrix} f_1\left[K_p^{11}K_i^{11}K_d^{11}\lambda^{11}\mu^{11} \; K_p^{12}K_i^{12}K_d^{12}\lambda^{12}\mu^{12} \; \ldots \; K_p^{1m}K_p^{1m}K_d^{1m}\lambda^{1m}\mu^{1m}\right] \\ f_2\left[K_p^{21}K_i^{21}K_d^{21}\lambda^{21}\mu^{21} \; K_p^{22}K_i^{22}K_d^{22}\lambda^{22}\mu^{22} \ldots \; K_p^{2m}K_i^{2m}K_d^{2m}\lambda^{2m}\mu^{2m}\right] \\ \vdots\vdots\vdots \\ f_n\left[K_p^{n1}K_i^{n1}K_d^{n1}\lambda^{n1}\mu^{n1} \; K_p^{n2}K_i^{n2}K_d^{n2}\lambda^{n2}\mu^{n2} \; \ldots K_p^{nm}K_i^{nm}K_d^{nm}\lambda^{nm}\mu^{nm}\right] \end{bmatrix} \tag{43}$$

The objective function is to get a comfortable air temperature and humidity by low energy consumption optimal tuning of FOPID controller using hybrid BOANFIST algorithm.

$$\min j(k) = \min(j_1(k) + j_2(k) + j_3(k)) \tag{44}$$

The values of $j_1(k), j_2(k), j_3(k)$ are expressed as

$$j_1(k) = \sum_k^{k+N_p} \left\| y_1(k) - T_{csr}(k) \right\|_{Q_r} \tag{45}$$

$$j_2(k) = \sum_k^{k+N_p} \left\| y_2(k) - W_{csr}(k) \right\|_{Q_r} \tag{46}$$

$$j_3(k) = \sum_k^{k+N_p} \left\| u(k) \right\|_{Q_u} \tag{47}$$

where T_{csr} refers to reference air temperature, W_{csr} refers to reference moisture content in conditioning room and y_1 , y_2 refer forecasted temperature and humidity of the *kth* step. The $j_1(k)$ denotes the indoor temperature deviation as its value of the set-point, $j_2(k)$ denotes the indoor humidity deviation and $j_3(k)$ denotes ramping rate of compressor speed.

Step 4: New Position Updation with ANFIS

The fuzzy rule is the preliminary step, the input variables determination and fuzzification. Each node j represents as adaptive functions of node is explained on this layer.

$$O_j^1 = \mu^{A_j}(X), j = 1, 2 \tag{48}$$

where input for jth node denoting X is associated. Therefore, membership in fuzzy sets (A_1, A_2) is denoted as O_j^1 and subsequent input X is fulfilled using quantifier A.

Step 5: Estimation of Membership Function

The function of membership for fuzzifying based on the Bell function is denoted in Eq. (49):

$$\mu_{A_j}(x_1) = \frac{1}{1 + \left(\frac{x - d_j}{a_j}\right)} \tag{49}$$

where d_j and a_j are the Bell function parameters.

Step 6: Estimation of Firing Strength

The layer 3 is demonstrated using "M" as circle node. Moreover, firing strength of every rule is estimated on this layer. The layer of output denotes is shown below:

$$O_j^2 = W_j = \mu^{A_j}(X) \cdot \mu^{B_j}(Y) \; for \; j = 1, 2 \tag{50}$$

Step 7: Normalization

Each T-norm operator performs fuzzy and operation on this layer. Every node is declared as "N" in layer 4. Output node is O_j^3 *or* $\overline{W_j}$ and it is calculated as follows:

$$O_j^3 = \overline{W_j} = \frac{W_j}{W_1 + W_2}, j = 1, 2 \tag{51}$$

Step 8: De-Fuzzification

In layer 5, each node is adaptive square node by node function, which is given in Eq. (52):

$$O_j^4 = \overline{W_j} \cdot f_j = \overline{W_j} \cdot \left(p_j x + q_j y + r_j\right) \; j = 1, 2 \tag{52}$$

Step 9: Tuning the FOPID Parameters

In layer 6, the single node estimates the total number of the entire received signals from layer 6 for producing the overall outcome. Here, ANFIS output is similar to the unique node. The output of the ANFIS structure for tuning the FOPID controller parameters to attain the adaptable indoor air temperature and humidity is given below:

$$O_j^5 = f = \sum_j W_j f_j = \frac{\sum_j W_j \cdot f_j}{\sum_j W_j} \tag{53}$$

In this manner, for a Sugeno fuzzy inference system, an adaptive network is nearly equal. The structure of ANFIS is shown in Fig. 3.

Step 10: Termination

The aforementioned process is completed when optimal results are attained using the goal function. In addition to the initialization phase, the preceding steps are repeated iteratively until a final base is met. Figure 4 depicts the established algorithm's flow chart.

5. RESULT AND DISCUSSION

A novel BOANFIST hybrid technique is proposed in this paper for concurrent control of indoor air temperature and humidity on DXA/C system with FOPID. To achieve the desired responses, FOPID controller gain is rotated through

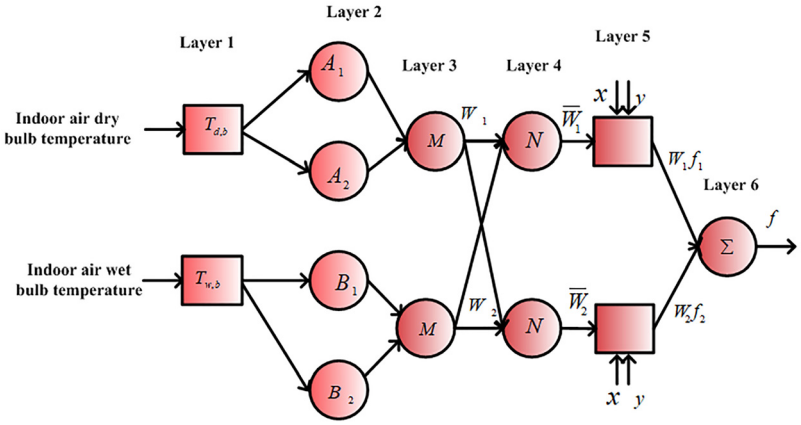

Fig. 3. Structure of the ANFIS

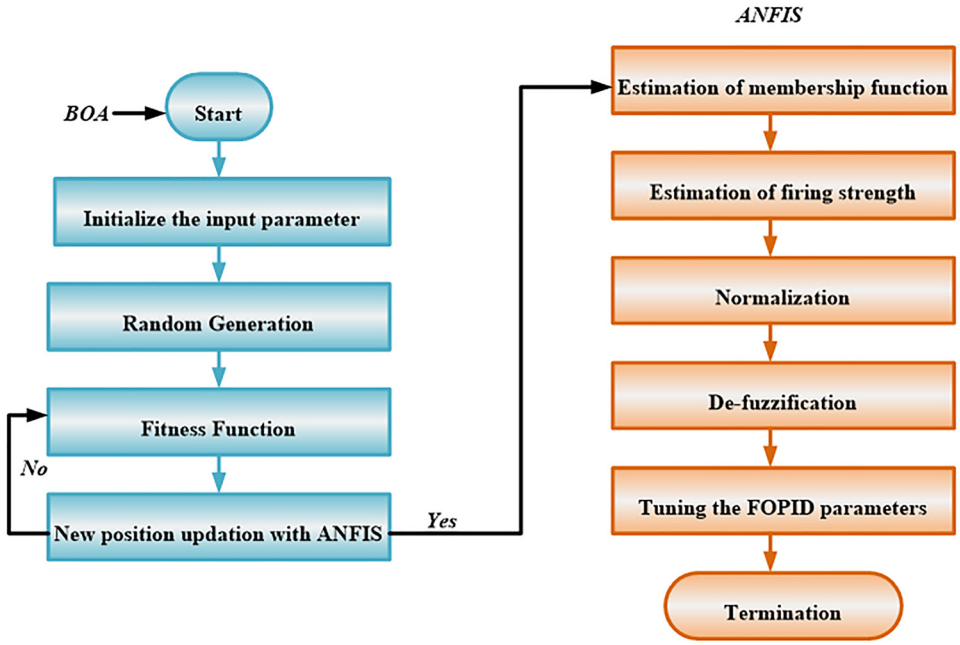

Fig. 4. Flowchart of the proposed hybrid BOANFIS algorithm

the ANFIS approach and RDF weight matrices are predictable with the help of the BOA method. The proposed BOANFIST technique guarantees the system stability under large disturbances with the reduction of the overshoot and the computation. The BOANFIST model is performed on MATLAB/Simulink platform. The results obtained are linked with some of the current methods, such as BOA, GOA and CS. The simulation parameters are shown in Table 1.

To achieve the enhanced performance of the proposed hybrid system, control parameters are carefully adjusted in simulation. The adjustment parameter is set to 0.5 and sampling interval 2 s. The pressure value of the condensation and evaporation is considered as 1.812×106 Pa and 0.486×106 Pa. Furthermore, the water vaporization latent

Table 1. Simulation parameters

Parameters	Ratings
C_{sa}	1.005 kJ kg^{-1}
δ	1.2 kg/m^2
V^*_{h1}	0.04 m^3
V^*_{h2}	0.16 m^3
h^*_{fg}	2,450 kJ kg^{-1}
V^*	77 m^3
P^*_c	1.812×10^6 Pa
β_1	0.0934 kW m^{-2} °C^{-1}
β_2	0.0457 kW m^{-2} °C^{-1}
A_1	4.14 m^2
A_2	17.65 m^2
P^*_e	0.486×106 Pa

heat value is taken as 2,450 kJ/kg and the coefficient of the heat transfer value is 0.0934 kW m^{-2} $°C^{-1}$ and 0.0457 kW m^{-2} $°C^{-1}$. These values provide better control performance and lead to a very easy atmosphere for indoors depending on the proposed system. It consists of numerous ways of restrictions on this DX A/C system. The matrices are taken as 23, 23, 23, 15, 12.44/1,000, 13.5/1,000 and 0.001. It is considered as 0.0415, 0.309 and 0.7. The output performance of the proposed hybrid BOANFIS method is illustrated in Fig. 4. At time 0–50 s, the system efficiency is slowly maximized. From this, the indoor humidity and air temperature can achieve their set points after working with the DX A/C system. The Bode diagram of the proposed system is displayed in Fig. 5.

The error of the proposed BOANFIST approach is demonstrated in Fig. 6. The proposed system error is gradually decreased at 0–50 s. After 250 s, the proposed system error is preserved at constant value. The overall performance analysis of the BOANFIST technique is expressed in Fig. 7. It indicates that the output of the proposed system is enhanced via the BOANFIST approach. Furthermore, the error of the system is gradually reduced. The convergence curve for the proposed hybrid BOANFIST method is shown in Fig. 8.

The proposed system accomplishes 1.69 convergence values. Besides, the overall performance analysis of the conventional CS system is displayed in Fig. 9. Overall

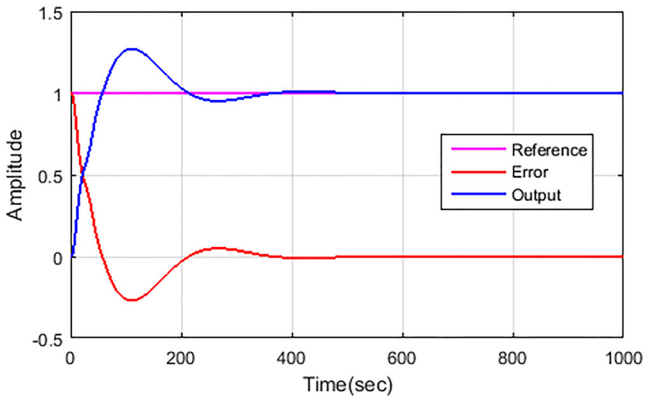

Fig. 7. Performance of proposed system

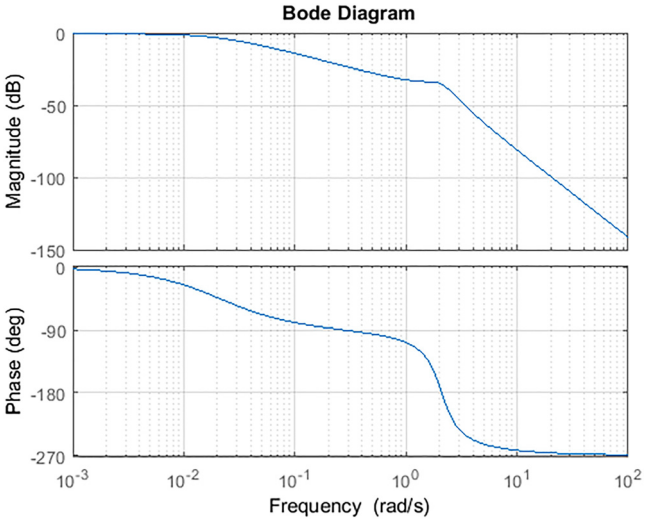

Fig. 5. Bode plot

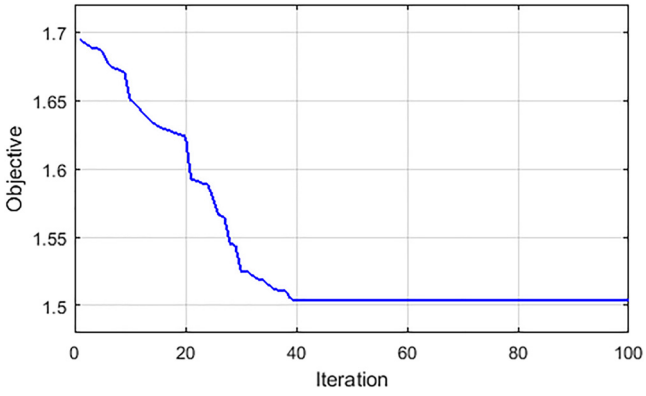

Fig. 8. Convergence curve for proposed system

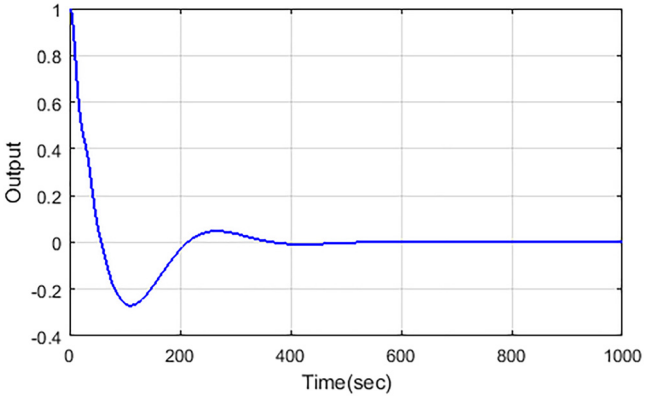

Fig. 6. Error of proposed system

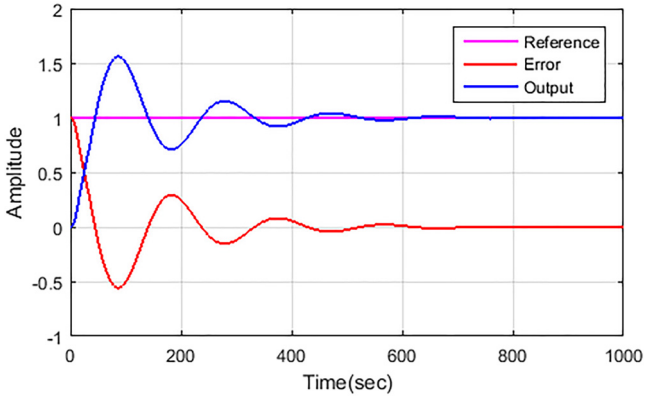

Fig. 9. Performance of CS system

performance analysis of conventional BOA system is demonstrated in Fig. 10. Furthermore, overall performance analysis of conventional GOA technique is displayed in Fig. 11. Overall comparison of proposed output performance to existing system is demonstrated in Fig. 12. The proposed system enhanced the output performance in less time when contrasted to the existing BOA, CS and GOA approaches. The overall error comparison of BOANFIST system with existing system is demonstrated in Fig. 13. Figure 14 portrays convergence comparison of the BOANFIST and existing system. The convergence of BOANFIST system results 1.69. The value of the convergence curve of BOA, CS and GOA system implies 1.75, 1.85 and 1.787. Likened to existing ones, the value of the BOANFIST hybrid method is less.

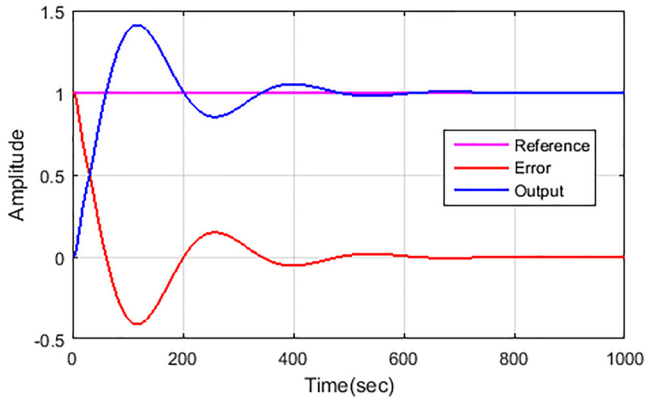

Fig. 10. Performance of BOA system

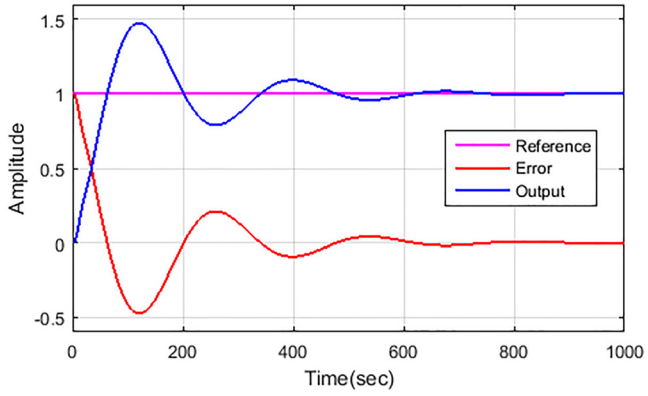

Fig. 11. Performance analysis of GOA system

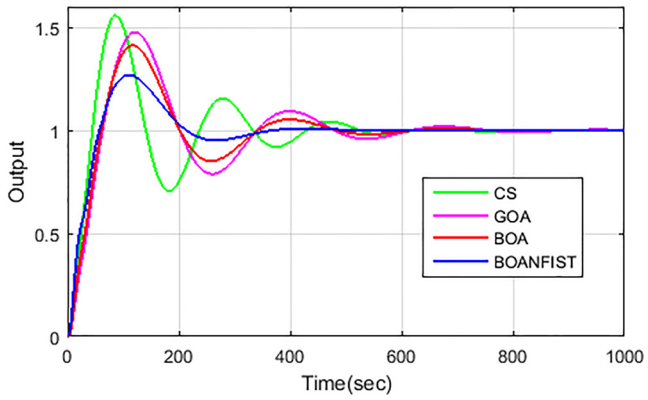

Fig. 12. Comparison of output performance with existing system

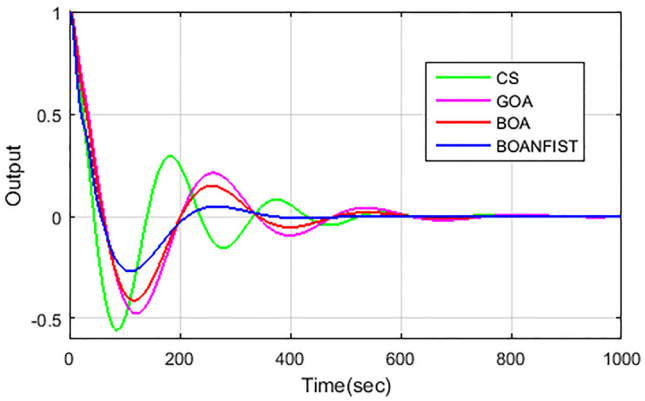

Fig. 13. Comparison of BOANFIST error with existing system

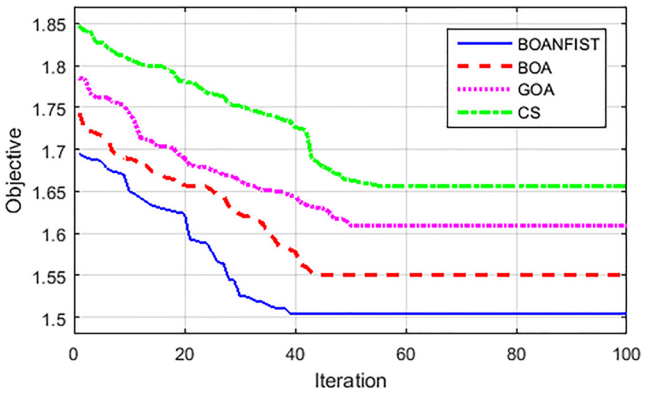

Fig. 14. Convergence comparison of BOANFIST and existing systems

Besides, the computational time comparison of BOANFIST and existing systems are represented in Fig. 15. The proposed BOANFIST approaches control the DXA/C system in less computation time. Computational time of BOA, GOA, and CS is 1.1 s, 1.2 s, and 1.23 s. Furthermore, the

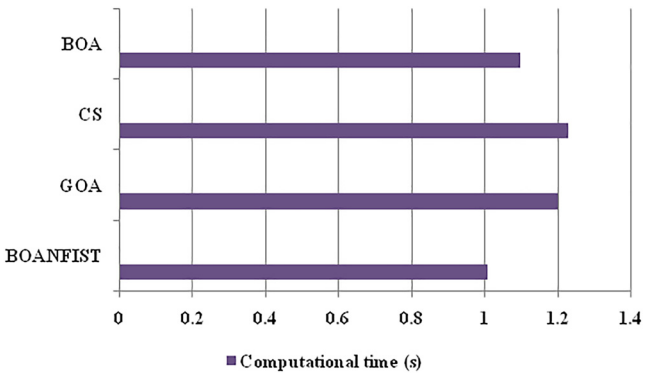

Fig. 15. Comparison of BOANFIST and existing systems

accuracy comparison of BOANFIST with existing method is portrayed in Fig. 16. The proposed system attains 99.69% accuracy which is high when compared with the conventional approaches.

$$P^*_{rec} = \frac{TP^*}{TP^* + FP^*} \tag{54}$$

$$R^*_{ca} = \frac{TP^*}{TP^* + FN^*} \tag{55}$$

$$S^*_{pe} = \frac{TN^*}{TN^* + FP^*} \tag{56}$$

where TP^* and FP^* are the true and false positive as well as TN^*, FN^* mean true and false negative. BOANFIST and existing methods are shown in Fig. 17. The BOANFIST method attains 98% as well as 97.8%. The specificity comparison of BOANFIST and existing methods is portrayed in Fig. 18. The proposed method attains 97.8% recall value. Statistical analysis of BOANFIST and existing system is portrayed in Table 2. The mean value of the proposed system is 1.5420, the median is 1.5043 and standard deviation is 0.0509. The error comparison for 50 trials of the proposed system with conventional system is portrayed in Table 3.

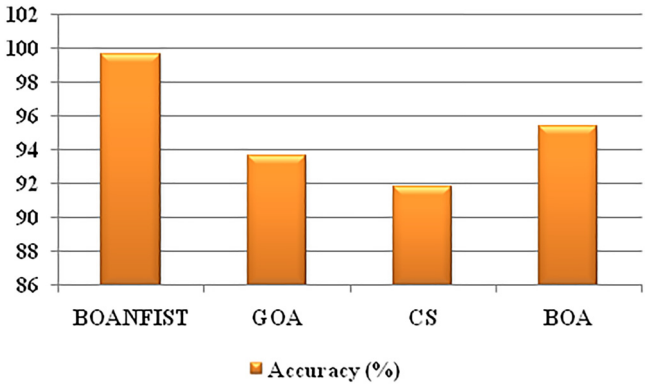

Fig. 16. Accuracy comparison of BOANFIST with existing techniques

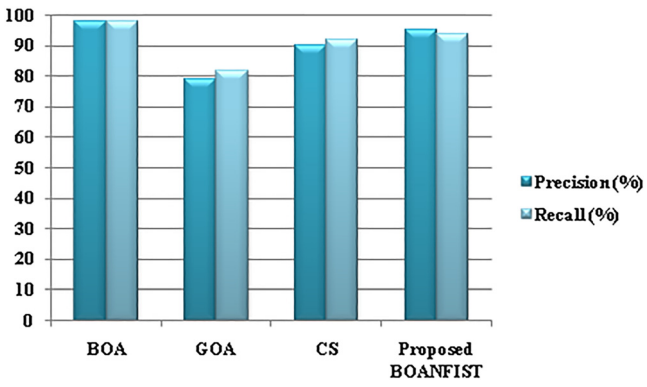

Fig. 17. Recall and precision comparison of BOANFIST and existing methods

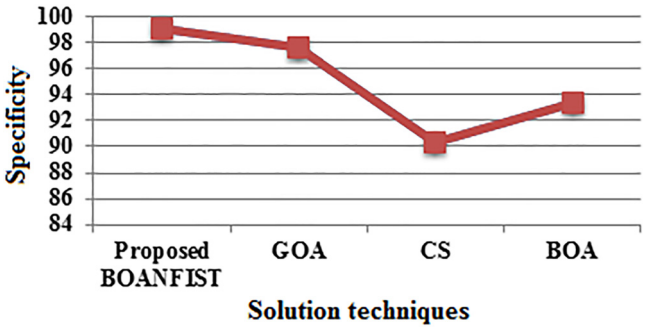

Fig. 18. Specificity comparison of BOANFIST with existing methods

Table 2. Statistic measures of BOANFIST and existing systems

Technique	Mean	Median	S.D
BOANFIST	1.5420	1.5043	0.0509
BOA	1.5930	1.5502	0.0588
GOA	1.6467	1.6095	0.0617
CS	1.7096	1.6628	0.0635

The BOANFIST system accomplishes 0.01103 RMSE value. The BOANFIST system diminishes IAE, ITAE, and ISE to 0.0215, 0.000279 and 0.0002157 for 50 numbers of trials. Besides, the error comparison for 100 trials of the proposed system and conventional system is demonstrated in Table 4. Furthermore, the BOANFIST and existing systems is articulated in Table 5. The BOANFIST system accomplishes the value of 0.99 and 0.979. Furthermore, energy consumption of the proposed system is low. Smaller indoor sensible cooling load resulted in lower consumption of energy through the air conditioner. In conclusion, the proposed technique provide better outcomes than the existing method.

Table 3. Error comparison of BOANFIST and existing methods for 50 number of trials

Method	RMSE	IAE	ITAE	ISE
BOA	0.0191	0.06327	0.001549	0.003392
GOA	0.0211	0.02633	0.0003478	0.0002656
CS	0.0134	0.03827	0.00129	0.00378
Proposed BOANFIST	0.01102	0.0214	0.000278	0.0002156

Table 4. Error comparison of BOANFIST and existing methods for 100 number of trials

Method	RMSE	IAE	ITAE	ISE
BOA	0.0234	0.0801	0.00278	0.00523
GOA	0.0366	0.0462	0.000427	0.000298
CS	0.0344	0.0428	0.00202	0.00393
Proposed BOANFIST	0.01981	0.0231	0.000328	0.000267

Table 5. Performance comparison of BOANFIST and existing approaches

Method	Computational time (s)	Energy consumption (kWh/day)	Precision (%)	Recall (%)	Accuracy (%)	Specificity (%)
BOA	1.1	18.05	98	97.8	95.37	99.09
GOA	1.2	19.25	79	82	93.61	97.68
CS	1.23	21.82	90	92	91.78	90.34
Proposed BOANFIST	1.01	16.42	95	94	99.69	93.36

6. CONCLUSION

A hybrid BOANFIST system is proposed in this paper for the DX-A/C system control of the indoor air temperature and humidity with FOPID controller. The suggested hybrid technique is a joint execution of ANFIS as well as BOA. The FOPID controller parameters are adjusted via the ANFIS approach and the weight matrices were predictable by the help of BOA method. The proposed BOANFIST method guarantees the system stability under large disturbances. At this point, the proposed model was executed at MATLAB/Simulink working stage. As a result, the proposed hybrid BOANFIST system effectively controls the temperature and indoor air with minimal computation reducing the complexity of the algorithm.

Data availability: Data sharing does not relate to this article, as no novel data was created or investigated under this study.

Funding information: This research did not receive any particular grant from funding agencies in the public, commercial, or non-profit sectors.

REFERENCES

[1] Z. Li and S. Deng, "A DDC-based capacity controller of a direct expansion (DX) air conditioning (A/C) unit for simultaneous indoor air temperature and humidity control – Part I: control algorithms and preliminary controllability tests," *Int. J. Refrigeration*, vol. 30, no. 1, pp. 113–23, 2007.

[2] T. Aynur, Y. Hwang, and R. Radermacher, "Simulation of a VAV air conditioning system in an existing building for the cooling mode," *Energy and Buildings*, vol. 41, no. 9, pp. 922–9, 2009.

[3] Q. Qi and S. Deng, "Multivariable control of indoor air temperature and humidity in a direct expansion (DX) air conditioning (A/C) system," *Building Environ.*, vol. 44, no. 8, pp. 1659–67, 2009.

[4] Q. Qi and S. Deng, "Multivariable control-oriented modeling of a direct expansion (DX) air conditioning (A/C) system," *Int. J. Refrigeration*, vol. 31, no. 5, pp. 841–9, 2008.

[5] Z. Li and S. Deng, "An experimental study on the inherent operational characteristics of a direct expansion (DX) air conditioning (A/C) unit," *Building Environ.*, vol. 42, no. 1, pp. 1–10, 2007.

[6] Q. Qi, S. Deng, X. Xu, and M. Chan, "Improving degree of superheat control in a direct expansion (DX) air conditioning (A/C) system," *Int. J. Refrigeration*, vol. 33, no. 1, pp. 125–34, 2010.

[7] X. Xu, L. Xia, M. Chan, and S. Deng, "Inherent correlation between the total output cooling capacity and equipment sensible heat ratio of a direct expansion air conditioning system under variable-speed operation (XXG SMD SHR DX AC unit)," *Appl. Therm. Eng.*, vol. 30, no. 13, pp. 1601–7, 2010.

[8] N. Li, L. Xia, D. Shiming, X. Xu, and M. Chan, "Dynamic modeling and control of a direct expansion air conditioning system using artificial neural network," *Appl. Energy*, vol. 91, no. 1, pp. 290–300, 2012.

[9] X. Xu, S. Deng, and M. Chan, "A new control algorithm for direct expansion air conditioning systems for improved indoor humidity control and energy efficiency," *Energy Convers. Manage.*, vol. 49, no. 4, pp. 578–86, 2008.

[10] D. Shiming, L. Zheng, and Q. Minglu, "Indoor thermal comfort characteristics under the control of a direct expansion air conditioning unit having a variable-speed compressor and a supply air fan," *Appl. Therm. Eng.*, vol. 29, nos 11–12, pp. 2187–93, 2009.

[11] N. Li, L. Xia, D. Shiming, X. Xu, and M. Chan, "On-line adaptive control of a direct expansion air conditioning system using artificial neural network," *Appl. Therm. Eng.*, vol. 53, no. 1, pp. 96–107, 2013.

[12] S. Lakshmanaprabu, M. Elhoseny, and K. Shankar, "Optimal tuning of decentralized fractional order PID controllers for TITO process using equivalent transfer function," *Cogn. Syst. Res.*, vol. 58, pp. 292–303, 2019.

[13] Z. Li, X. Xu, S. Deng, and D. Pan, "A novel proportional-derivative (PD) law based fuzzy logic principles assisted controller for simultaneously controlling indoor temperature and humidity using a direct expansion (DX) air conditioning (A/C) system," *Int. J. Refrigeration*, vol. 57, pp. 239–56, 2015.

[14] Z. Li, X. Xu, S. Deng, and D. Pan, "Further study on the inherent operating characteristics of a variable speed direct expansion air conditioning system," *Appl. Therm. Eng.*, vol. 66, nos 1–2, pp. 206–15, 2014.

[15] L. Yang, H. Yan, S. Deng, and W. Li, "An experimental investigation on the operational characteristics of a novel direct expansion based air conditioning system with a two-sectioned cooling coil," *Int. J. Refrigeration*, vol. 118, pp. 131–8, 2020.

[16] Y. Xia, Q. Ding, Z. Jiang, S. Deng, and M. Song, "Development of a superheat controller for mitigating hunting in a direct expansion air conditioning system," *Energy Proced.*, vol. 158, pp. 2085–91, 2019.

[17] F. H. Shajin, P. Rajesh, and S. Thilaha, "Bald eagle search optimization algorithm for cluster head selection with prolong lifetime

in wireless sensor network," *J. Soft Comput. Eng. Appl.*, vol. 1, no. 1, p. 7, 2020.

[18] P. Rajesh, F. H. Shajin, and L. Umasankar, "A novel control scheme for PV/WT/FC/Battery to power quality enhancement in micro grid system: a hybrid technique," *Energy Sourc. A: Recovery, Utilization, Environ. Effects*, pp. 1–17, 2021.

[19] F. H. Shajin and P. Rajesh, "FPGA realization of a reversible data hiding scheme for 5G MIMO-OFDM system by chaotic key generation-based paillier cryptography along with LDPC and its side channel estimation using machine learning technique," *J. Circuits, Syst. Comput.*, 2021, Paper no. 2250093.

[20] P. Rajesh, F. H. Shajin, B. Mouli Chandra, and B. N. Kommula, "Diminishing energy consumption cost and optimal energy management of photovoltaic aided electric vehicle (PV-EV) by GFO-VITG approach," *Energy Sourc. Part A: Recovery, Utilization, Environ. Effects*, pp. 1–19, 2021.

[21] Y. Xia, S. Deng, and M. Chan, "Inherent operational characteristics and operational stability of a variable speed direct expansion air conditioning system," *Appl. Therm. Eng.*, vol. 113, pp. 268–77, 2017.

[22] X. Xiangguo, P. Yan, D. Shiming, X. Liang, and C. Mingyin, "Experimental study of a novel capacity control algorithm for a multi-evaporator air conditioning system," *Appl. Therm. Eng.*, vol. 50, no. 1, pp. 975–84, 2013.

[23] V. Vakiloroaya, B. Samali, and K. Pishghadam, "Investigation of energy-efficient strategy for direct expansion air-cooled air conditioning systems," *Appl. Therm. Eng.*, vol. 66, nos 1–2, pp. 84–93, 2014.

[24] H. Yan, S. Deng, and M. Chan, "A novel capacity controller for a three-evaporator air conditioning (TEAC) system for improved indoor humidity control," *Appl. Therm. Eng.*, vol. 98, pp. 1251–62, 2016.

[25] Q. Yang, J. Zhu, X. Xu, and J. Lu, "Simultaneous control of indoor air temperature and humidity for a chilled water based air conditioning system using neural networks," *Energy and Buildings*, vol. 110, pp. 159–69, 2016.

[26] Y. Xia, Q. Ding, S. Jiangzhou, X. Zhang, and S. Deng, "A simulation study on the operational stability of an EEV-controlled direct expansion air conditioning system under variable speed operation," *Int. J. Refrigeration*, vol. 103, pp. 115–25, 2019.

[27] K. O. Sholahudin, N. Giannetti, S. Yamaguchi, and K. Saito, "Dynamic modeling of room temperature and thermodynamic efficiency for direct expansion air conditioning systems using Bayesian neural network," *Appl. Therm. Eng.*, vol. 158, 2019, Paper no. 113809.

[28] H. Tang, T. Zhang, and X. Liu, "Experimental study on refrigerant maldistribution in a fin-and-tube evaporator for a direct expansion air-conditioning system," *Energy and Buildings*, vol. 208, 2020, Paper no. 109638.

[29] J. Xie, Y. Pan, W. Jia, L. Xu, and Z. Huang, "Energy-consumption simulation of a distributed air-conditioning system integrated with occupant behaviour," *Appl. Energy*, vol. 256, 2019, Paper no. 113914.

[30] H. Yan, Y. Xia, X. Xu, and S. Deng, "Inherent operational characteristics aided fuzzy logic controller for a variable speed direct expansion air conditioning system for simultaneous indoor air temperature and humidity control," *Energy and Buildings*, vol. 158, pp. 558–68, 2018.

[31] H. Yan, Y. Pan, Z. Li, and S. Deng, "Further development of a thermal comfort based fuzzy logic controller for a direct expansion air conditioning system," *Appl. Energy*, vol. 219, pp. 312–24, 2018.

[32] W. Chen, M. Chan, S. Deng, H. Yan, and W. Weng, "A direct expansion based enhanced dehumidification air conditioning system for improved year-round indoor humidity control in hot and humid climates," *Building Environ.*, vol. 139, pp. 95–109, 2018.

[33] P. Bahramnia, S. HosseiniRostami, J. Wang, and G. Kim, "Modeling and controlling of temperature and humidity in building heating, ventilating, and air conditioning system using model predictive control," *Energies*, vol. 12, no. 24, p. 4805, 2019.

[34] W. Kang, W. H. Kang, J. M. Lee, S. H. Yeon, M. K. Park, C. H. Kim, J. H. Lee, J. W. Moon, and K. H. Lee, "Modeling, calibration, and sensitivity analysis of direct expansion AHU-Water source VRF system," *Energy*, vol. 199, 2020, Paper no. 117435.

[35] H. Yan, Y. Xia, and S. Deng, "Adaptive control for degree of refrigerant superheat in a direct expansion air conditioning system under variable speed operation," *Energy Proced.*, vol. 158, pp. 2182–7, 2019.

[36] F. Muñoz, E. Sanchez, Y. Xia, and S. Deng, "Real-time neural inverse optimal control for indoor air temperature and humidity in a direct expansion (DX) air conditioning (A/C) system," *Int. J. Refrigeration*, vol. 79, pp. 196–206, 2017.

[37] J. Mei and X. Xia, "Energy-efficient predictive control of indoor thermal comfort and air quality in a direct expansion air conditioning system," *Appl. Energy*, vol. 195, pp. 439–52, 2017.

[38] Z. Zhong, X. Xu, X. Zhang, and Z. Huang, "Simulation based control performance evaluation of a novel fuzzy logic control algorithm for simultaneously controlling indoor air temperature and humidity using a direct expansion (DX) air-conditioning (A/C) system," *Proced. Eng.*, vol. 205, pp. 1792–9, 2017.

[39] M. Micev, M. Ćalasan, and D. Oliva, "Fractional order PID controller design for an AVR system using chaotic yellow saddle goatfish algorithm," *Mathematics*, vol. 8, no. 7, p. 1182, 2020.

[40] S. Arora and S. Singh, "Butterfly optimization algorithm: a novel approach for global optimization," *Soft Comput.*, vol. 23, no. 3, pp. 715–34, 2018.

[41] A. Kheirandish, E. Akbari, M. Nilashi, and M. Dahari, "Using ANFIS technique for PEM fuel cell electric bicycle prediction model," *Int. J. Environ. Sci. Technol.*, vol. 16, no. 11, pp. 7319–26, 2019.